SAND2017-6571C

Parametric PV Grid-Support Function Characterization for Simulation Environments

Javier Hernandez-Alvidrez[1], and Jay Johnson[2]

[1]New Mexico State University, Las Cruces, New Mexico, 88003, USA.
[2]Sandia National Laboratories, Albuquerque, New Mexico, 87185,USA

***Abstract*—Modern photovoltaic (PV) inverters and other inverter-based distributed energy resources (DER) have the ability to provide grid-support capabilities with different advanced inverter functions. At this time, the nuanced influence of these functions on many grid operations, such as voltage regulation, frequency reserve deployment, protection systems, and other ancillary services is not fully understood. Researchers are increasingly turning to hardware-in-the-loop (HIL) simulations to answer these questions by coupling physical devices to power simulations. Unfortunately, it is common for these simulations to use ideal power converter models to represent the end-devices. In this paper, we perform parametric characterization of multiple PV inverter products to generate empirical equations which accurately describe the inverter behavior for volt-var, fixed power factor, and frequency-watt grid support functions over a range of operating conditions. These equations can then be used in HIL and other power simulations to better represent the actual output of fielded equipment.**

***Index Terms*—inverters, hardware in the loop, volt-var, frequency-watt, fixed power factor, inverter model.**

I. Introduction

In 2015, the California Public Utilities Commission joined Hawaii and a number of European jurisdictions requiring grid-support functionality from PV inverters [1]–[4]. A large effort is also currently underway to revise the national interconnection standard, IEEE Std. 1547 [5], to require additional distributed energy resource (DER) grid-support functions and device interoperability. The new functions required in these standards have the ability to assist grid operators to perform voltage regulation, frequency stabilization, power system protection via different operating modes.

The combination of modes (i.e. grid support functions) and settings for specific use cases with a given circuit topology and collection of DER assets is widely studied in the literature. Typically these studies rely on power simulations to determine the optimal settings for the given scenario. In many power simulations, the advanced-grid functions are modeled as ideal functions without measurement inaccuracies, generation errors, or time delays. For instance, studies of voltage regulation [6] and hosting capacity using the volt-var function [7] assume perfect reactive power generation for a given grid voltage production. However, physical devices can have significant errors in ideal behavior and response times can be lengthy [8]–[12]. The results of advanced grid function tests conducted by the Smart Grid International Research Facility Network (SIRFN) for PV [13] and energy storage systems [14] found large errors for some devices. The latency of the frequency-watt function was found to be detrimental to providing fast contingency reserves [9], [14]; and communication latencies with fixed power factor and constant reactive power were found to disrupt voltage regulation control strategies [6]. And recently, miscalculated frequencies from inverters caused approximately 700 MW of generation to trip in the Western Interconnection [15].

In the U.S., grid-interconnected DER assets are tested to the Underwriters Laboratories (UL) 1741 [16] certification standard by a Nationally Recognized Testing Laboratory (NRTL). The most recent version of UL 1741 was published in 2016 and includes a test procedure to evaluate and certify DER grid-support functions in Supplement A. The current language allows vendors to certify products that fall within the manufacturer's specified accuracy, unless specifically called out in the interconnection source requirements document (SRD)– e.g. CA Rule 21, HI Rule 14H, IEEE 1547. Most of the SRDs do not specify accuracies for the grid support functions so inverter manufacturers are free to provide generous accuracies in order to pass the tests. As a result, the DER may not behave as programmed in the field and, as a result, grid operators may not correctly select the DER settings or functions to provide grid services.

In response, researchers are increasingly employing control hardware-in-the-loop (CHIL) and power hardware-in-the-loop (PHIL) techniques to better understand how equipment will operate in the field [3]. Yet, for large HIL power system simulations, DER devices are typically modeled as ideal converters. In this work, we seek to establish a methodology for representing physical PV inverters as analytical models to accurately capture grid-support function behavior. In order to provide recommendations on the types of models which most accurately represent the response of the equipment, we generate and compare models of two PV inverters from different vendors under a range of PV irradiance conditions with fixed power factor, volt-var, and freq-watt functions.

II. Experimental Configuration

In order to assess the DER for a range of operating conditions and functions, the SunSpec System Validation Platform (SVP) [17] was used to communicate to an Ametek RS-180 180 kVA grid simulator, a 200 kW Ametek PV Simulator, National Instruments PCIe-6259 data acquisition cards, and

the Equipment Under Test (EUT). The test configuration is shown in Fig 1.

The advanced grid-support functions were configured in the EUT through SunSpec Modbus RTU or TCP commands. The grid voltage and PV irradiance were set via communications to the grid and PV simulators using the SVP scriptable interface. The IV curve of the PV simulator was programmed to provide nameplate EUT power at 1000 W/m^2 irradiance. At 1000 W/m^2 the EUT operated just under its AC nameplate power because of the device efficiency. For each setting, six cycles of the current and voltage waveforms were captured at 10 kHz via the National Instruments (NI) data acquisition system and processed for parameters of interest using the IEEE Std. 1459 [18]. Experiments were conducted for the support functions implemented in two inverters from different manufacturers labeled hereafter as EUT A and EUT B.

A. Volt-Var Function

For each of the inverters, the steady-state volt-var behavior of the EUTs was determined after a 2 second settling time. Grid voltages were evenly sampled 250 times (or every ~0.2 V) from V_{min} to V_{max} (the low and high voltage trip points) of the EUTs to fully characterize the curves. The curves were swept in increasing and decreasing voltage directions to capture any hysteresis at irradiance values of 100-1100 W/m^2 at 100 W/m^2 increments. Three Volt/Var curves were programmed into the devices to evaluate different VV settings.

B. Fixed Power Factor

The fixed power factor function was tested on the two EUTs at incremental values of 0.01 from PF_{min} to PF_{max}. At each power factor setting the irradiance values were adjusted from 100-1100 W/m^2 at 100 W/m^2 increments.

C. Frequency-Watt Function

The freq-watt function was evaluated on the two inverters by adjusting the grid simulator frequency from 59.5 to 62.0 Hz at irradiance values of 100-1000 W/m^2 at 100 W/m^2 increments.

III. Analytical Models

The proposed analytical inverter model is of the form:

$$Y\left[P,Q\right] = \sum a_i \cdot f_i \tag{1}$$

where Y is the active or reactive power output of the EUT (P or Q), a_i is a boolean representing function activation, and f_i is the inverter function. In this work we investigate the EUT response by considering three functions with the values of a_i being mutually exclusive, so the output of the inverter is represented by:

$$\begin{aligned} Y = P,Q = {} & a_{PF} \cdot f_{PF}\left(G, PF_{settings}\right) + \\ & a_{VV} \cdot f_{VV}\left(G, VV_{settings}, V_{grid}\right) + \\ & a_{FW} \cdot f_{FW}\left(G, FW_{settings}, F_{grid}\right) + \end{aligned} \tag{2}$$

where the analytical model of each function is expressed with a parametric mathematical expression that depends on three parameters: EUT settings, DC power conditions (PV irradiance), and grid conditions (f,V). Since we consider the response from each of these functions individually, e.g.

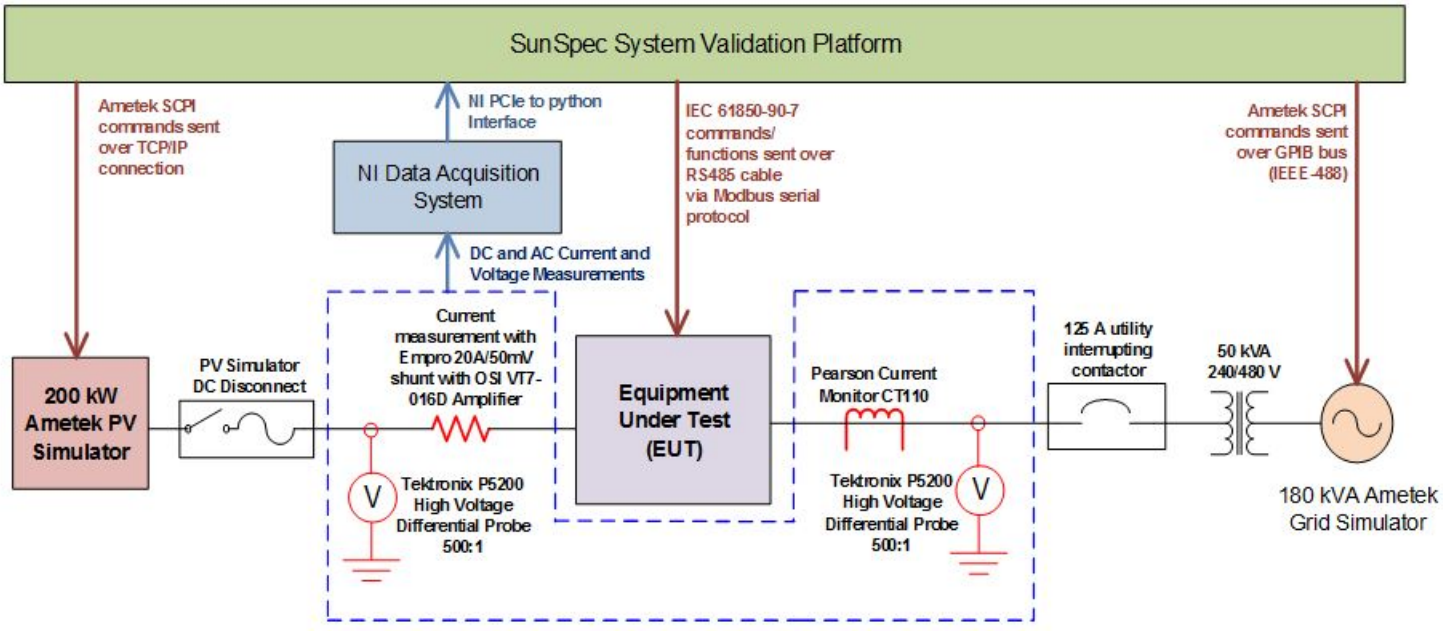

Fig. 1: Inverter Testbed at Sandia National Laboratories' Distributed Energy Technologies Laboratory (DETL).

only one a_i value can be 1 (true) at a time, then (2) can be expressed as:

$$Y = P, Q = \begin{bmatrix} a_{PF} & 0 & \\ 0 & a_{VV} & 0 \\ 0 & 0 & a_{FW} \end{bmatrix} \begin{bmatrix} f_{PF} \\ f_{VV} \\ f_{FW} \end{bmatrix} \tag{3}$$

In order to characterize the behavior of the aforementioned functions with analytical models, three different curve fitting approximation methods were evaluated: linear piecewise, polynomial interpolation, and Fourier approximation.

A. Linear Piecewise

In piecewise curve fitting method, the set of experimental data was approximated by a set of linear functions, where each function characterizes a particular section of the data on which the behavior can be modeled with a first order (linear) algorithm. This method proves to be quite effective in the approximation of functions with relatively long linear sections with sharp discontinuities between them, such as the ones encountered in the VV of FW functions. The general expression for this method is:

$$Y(x) = \begin{cases} A_1 \cdot x + B_1, \text{if } x_{1min} \leq x \leq x_{1max} \\ A_2 \cdot x + B_2, \text{if } x_{2min} \leq x \leq x_{2max} \\ \quad \vdots \\ A_n \cdot x + B_n, \text{if } x_{nmin} \leq x \leq x_{nmax} \end{cases} \tag{4}$$

where n is the number of linear sections used. Coefficients A and B depend on the type of linear interpolation used to characterize their respective linear section.

B. Polynomial Interpolation

With this method, the experimental set of data was approximated by means of an n order polynomial of the form:

$$Y(x) = a_0 + a_1 x + a_2 x^2 + ... + a_n x^n \tag{5}$$

Provided (5) passes through all ordinate values of the experimental ordered pairs: (x_0, y_0), (x_1, y_1), ...,(x_m, y_m), and m is the total number of pairs. Then, the coefficients of (5) can be obtained from:

$$\begin{bmatrix} a_0 \\ a_1 \\ \vdots \\ a_n \end{bmatrix} = \begin{bmatrix} 1 & x_0 & x_0^2 & \cdots & x_0^n \\ 1 & x_1 & x_1^2 & \cdots & x_1^n \\ \vdots & \vdots & \vdots & \ddots & \vdots \\ 1 & x_m & x_m^2 & \cdots & x_m^n \end{bmatrix}^{-1} \begin{bmatrix} 1 \\ y_0 \\ \vdots \\ y_n \end{bmatrix} \tag{6}$$

or, in a simplified way:

$$\vec{a} = \mathbf{V}(x) \cdot \vec{y} \tag{7}$$

where $\mathbf{V}(x)$ is called the Vandermonde matrix [19] and its dimension is determined by the total number of experimental ordered pair points (rows), and by the desired number of polynomial coefficients (columns). The higher the number of coefficients the higher the accuracy of the approximated polynomial at the expense of using more computational resources for coefficient calculation.

C. Fourier Approximation

In this approximation method the dynamics of the set of experimental data points is modeled as a linear combination of harmonically related sinusoids, which gives:

$$\begin{aligned} Y(x) =& A_0 + A_1 \sin(\omega x + \varphi_1) + A_2 \sin(2\omega x + \varphi_2) + ... \\ &+ A_n \sin(n\omega x + \varphi_n) \end{aligned} \tag{8}$$

where the coefficients (A_0 to A_n) and phase angles (φ_1 to φ_n) are obtained by applying the Discrete Fourier Transform [20] to the experimental set of data. As with the case of polynomial approximation, the more terms included in the model, the more accurate the approximation will be, but at the expense of using more computational resources to compute the Fourier coefficients and phase angles.

IV. Experimental Results

Figure 2 shows the experimental results of the Volt-Var curves implemented on EUT A and EUT B. In the figure, the programmed VV function is shown as a black solid line and each colored scatter plot represents the experimental data corresponding to a different irradiance level. From Fig.2, it can be observed that for each irradiance level in EUT A there is a systematic offset in both the voltage and the reactive power, clearly seen in the dead band of the VV curve. The offset in the AC voltage at the Point of Common Coupling (PCC) is most likely related to measurement error of the EUT. The voltage at the PCC was independently verified to within 0.1 V by a calibrated handheld meter and the calibrated NI DAQ system. The offset in the reactive power is most likely related to the output filter of the inverter. It can also be observed that the reactive power available is curtailed at lower irradiance levels, this is due to the power factor constraint of EUTA. Another way of visualizing the VV behavior of the EUT is to plot the results on an active-reactive power (P-Q) plane. As shown in Fig. 3, at low irradiance, the EUT holds the active power constant as the voltage changes the reactive power. At higher irradiance levels, the EUT adjusts active power as the voltage deviates from V_{nom}. The power factor ratings of EUTA ($\pm$0.85) and EUTB ($\pm$0.80) are shown with red lines. EUTA VV function is constrained to the PF limits of the equipment, but the reactive power of EUT B is limited by the reactive power limits of the device ($\pm$ 1600 VAr). This must be captured in the analytical model.

Figure 4 shows the experimental results of the fixed power factor function for EUT A and EUT B. The dynamics of the function were plotted in such a way that for each colored scattered plot the reactive power is a function of the DC irradiance level (independent variable) while keeping the power factor constant (parametric variable). From Fig. 4, it can be noticed an offset on the reactive power of EUT A for unity power factor, which directly correlates with the systematic offset in EUT A of Fig. 2. Visually, the dynamics of EUT B have a better behavior than EUT A. From Fig. 4 notice that the offset at unity power factor is very close to

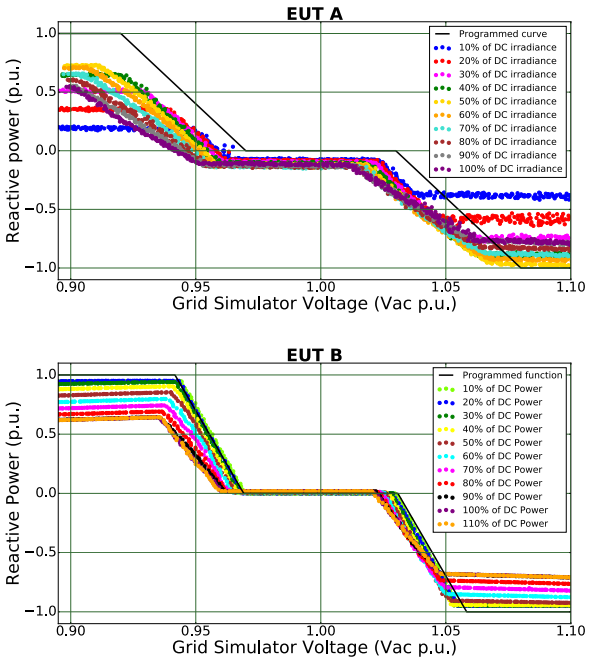

Fig. 2: Volt-Var curves.

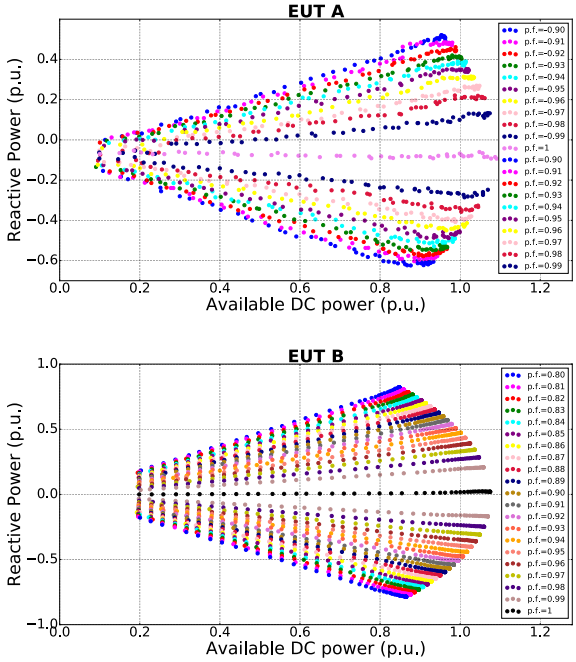

Fig. 4: Fixed power factor curves.

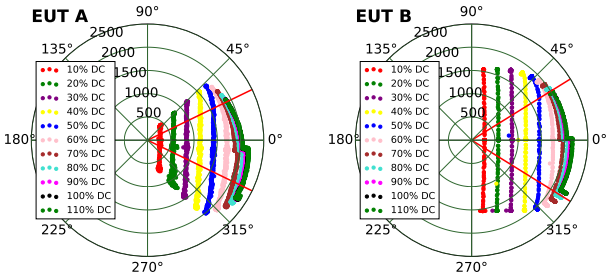

Fig. 3: EUT A and EUT B volt-var curves in the P-Q plane.

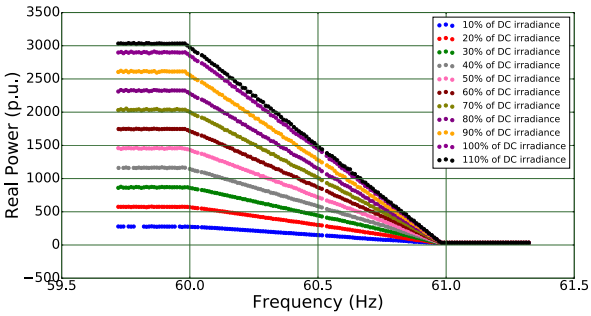

Fig. 5: Frequency-Watt curves for EUT B.

zero, and also the well defined linearity for each power factor waveform in EUT B compared to EUT A.

Figure 5 shows the experimental results of the FW curve for EUT A and B, where each colored scattered waveform corresponds to a different DC irradiance level.

V. Analytical Model Implementation

The three inverter functions were modeled using the aforementioned approximation methods. For each function, the implemented algorithm has three routines: (a) that extracts the experimental data and identifies the independent and parametric variables according to Table I, (b) that performs the approximation method, and (c) that interpolates between parametric data if the desired parametric variable G_{des} is not in the data sets.

A. *Volt-Var function*

The three approximations of the VV function for EUT B are shown in Fig. 6. For the linear piecewise approximation, the approximation curves (green curves) model the sharp corners with a good degree of accuracy. For the polynomial interpolation, which was approximated using n=53, the modeled function tracks the experimental data smoothly except for the sharp corners. In order to reduce the error to less than 1% in the sharp corners, a polynomial of at least 100th

TABLE I: Variable assignments for each function.

Inverter Function	Independent variable	Parametric variable
Volt-Var	Grid Voltage	DC irradiance
Fixed PF	DC irradiance	Power factor
Frequency-Watt	Grid Frequency	DC irradiance

order must be used, which not only significantly increases the computational resources needed, but may also lead to ill-conditioned polynomials [19]. For the Fourier approximation, 35 harmonically related sinusoids were used. The intrinsic oscillatory nature of this method appears at the ends of the curve in the form of high frequency oscillations although this high frequency variation could be reduced with a higher order Fourier approximation. Also, the sharp corners are modeled in a more accurate way compared to the polynomial interpolation.

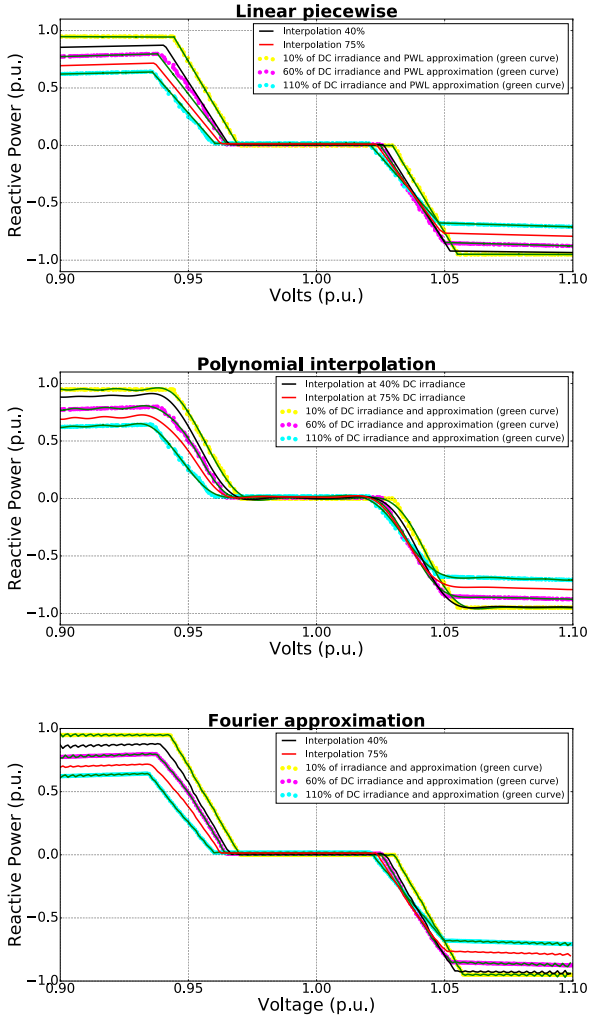

Fig. 6: Approximations of Volt-Var function for EUT B.

B. Fixed Power Factor

The results of the approximations function are shown in Fig. 7. This function was not modeled with the Fourier approximation method due to the lack of periodicity of the experimental results. The fitting performance of the two approximations of Fig. 7 was compared using the Pearson correlation coefficient (R^2). Therefore, based on R^2, the polynomial approximation seemed to be a better fit for this function. However, this approximation showed overfitting problems due to the roughly linear behavior of the experimental data, which means that the linear approximation can be expected to interpolate better.

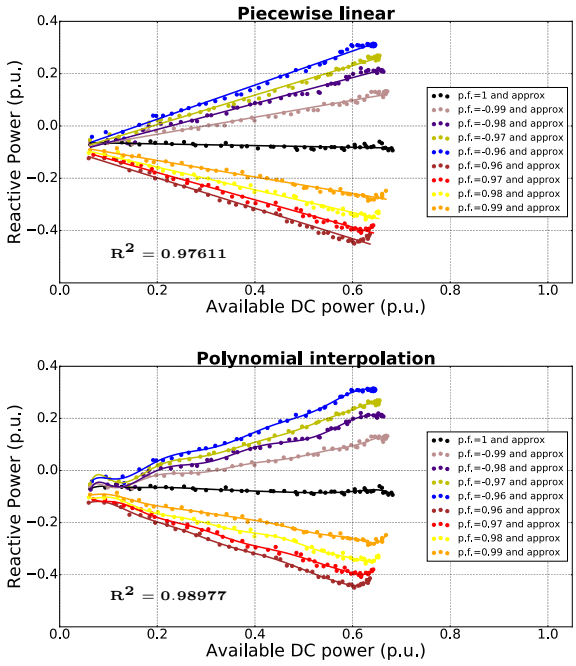

Fig. 7: Approximations of Fixed Power Factor functions for EUT A.

C. Frequency-Watt function

The results of the approximations curves for this function are shown in Fig. 8. Again, the piecewise linear method was the best option to model the sharp corners of the curve. Also, the polynomial interpolation and Fourier approximation were given the same number of terms as with the Volt-Var function (n=53 for polynomial, and 35 harmonically related terms for Fourier approximation), and since the Frequency-Watt curve has only 2 sharp corners, the accuracy of the approximation for this curve was improved at such sharp corners in comparison with the Volt-Var curve.

VI. CONCLUSIONS

In order to accurately represent inverters with grid-support functions in HIL simulations, a generalized inverter model was created. This model was represented with three different approximation methods and validated with three functions.

The piecewise linear approximation method proved to be suitable in terms of accuracy for curves with sharp corners as long as the data points of each section are linearly well-aligned. However, due to the sectionalized (non-continuous) nature of this method, interpolation between parameterized curves results is more difficult since the algorithm needs

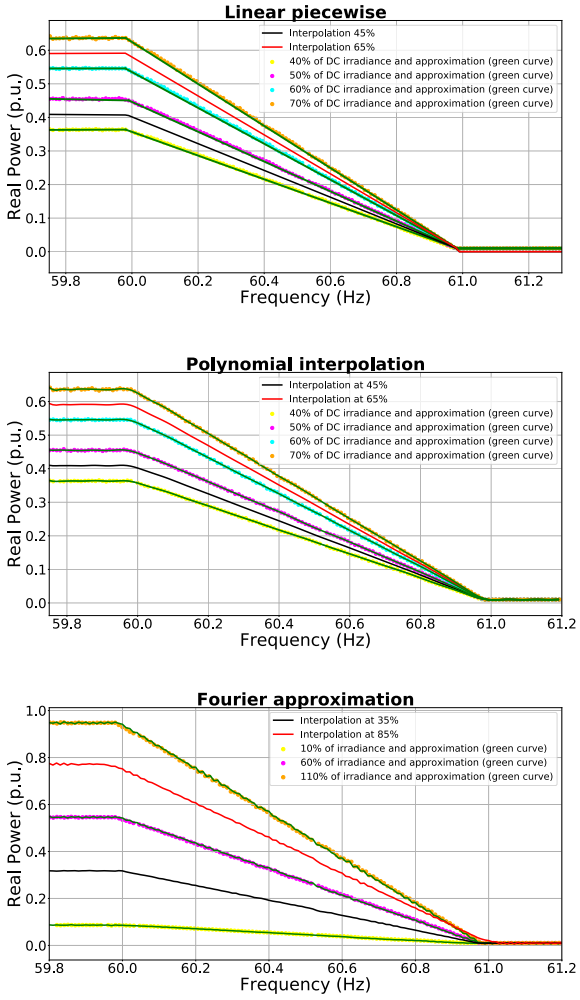

Fig. 8: Approximations of Frequency-Watt functions for EUT B.

significant amount of logic statements to identify the starting and ending points of each section of the curve for every single value of the independent variable.

The polynomial interpolation method proved to be effective in curves with scattered data points as well as curves with systematic offsets. But, this method lacked good accuracy in the neighborhood of sharp corners. The continuous nature of this method provided and easy way to interpolate between parameterized curves.

The Fourier method proved to be effective in complex curves like VV or FW. The accuracy of this method relies on the number of harmonically related components used to model the curves. Also, this method provided a much better accuracy in the neighborhood of sharp corners when compared to polynomial interpolation. The benefits of ease of interpolation of this method also apply due to its continuous nature.

VII. Acknowledgments

Sandia National Laboratories is a multi-mission laboratory managed and operated by National Technology and Engineering Solutions of Sandia, LLC., a wholly owned subsidiary of Honeywell International, Inc., for the U.S. Department of Energy's National Nuclear Security Administration under contract DE-NA-0003525.

References

[1] Pacific Gas and Electric Co, "Electric Rule No. 21, Generating Facility Interconnections, Filed with the CPUC," Jan. 20, 2015.

[2] Hawaiian Electric Company, "Inc. Rule No. 14, Service Connection and Facilities on Customers Premises, D&O No. 33258 filed Oct. 12, 2015, effective Oct 21, 2015."

[3] R. Bründlinger, T. Strasser, G. Lauss, A. Hoke, S. Chakraborty, G. Martin, B. Kroposki, J. Johnson, E. de Jong, "Lab Tests: Verifying That Smart Grid Power Converters Are Truly Smart," in *IEEE Power and Energy Magazine*, vol. 13, no. 2, March-April 2015, pp. 30–42. doi: 10.1109/MPE.2014.2 379 935.

[4] D. Rosewater, et al., "International development of energy storage interoperability test protocols for renewable energy integration," in *EU PVSEC, Hamburg, Germany*, Sept 14-18 2015.

[5] IEEE 1547 Std. 1547-2008, "IEEE Standard for Interconnecting Distributed Resources with Electric Power Systems," Institute of Electrical and Electronics Engineers, Inc. New York, NY, Standard, Sept 2008.

[6] M. J. Reno, J. E. Quiroz, O. Lavrova, R. H. Byrne, "Evaluation of communication requirements for voltage regulation control with advanced inverters," in *North American Power Symposium (NAPS)*. Denver, CO: IEEE, Sept 2016, pp. 1–6.

[7] J. Seuss, M. J. Reno, R. J. Broderick, S. Grijalva, "Improving Distribution Network PV Hosting Capacity via Smart Inverter Reactive Power Support," in *IEEE PES General Meeting*. Denver, CO: IEEE, July 2015.

[8] J. B. Ahn, J. J. Lee, J. Johnson, J. H. Bae, "Test Results for Advanced Inverter Functions Based-on IEC 61850-90-7," in *5th Asia-Pacific Forum on Renewable Energy (AFORE)*, Jeju, Korea, 4-7 November 2015.

[9] J. Neely, J. Johnson, J. Delhotal, S. Gonzalez, M. Lave, "Evaluation of PV Frequency-Watt Function for Fast Frequency Reserves," in *IEEE Applied Power Electronics Conference (APEC)*, Long Beach, CA, March 20-24 2016.

[10] S. Gonzalez, J. Johnson, J. Neely, "Electrical Power System Support-Function Capabilities of Residential and Small Commercial Inverters," in *42nd IEEE PVSC*, New Orleans, LA, June 14-18 2015.

[11] S. Gonzalez, J. Johnson, M. Reno, T. Zgonena, "Small Commercial Inverter Laboratory Evaluations of UL 1741 SA Grid-Support Function Response Times," in *43rd IEEE PVSC*, New Orleans, LA, June 5-10 2016.

[12] B. Seal, et al, "Final Report for CSI RD&D Solicitation #4 Standard Communication Interface and Certification Test Program for Smart Inverters," June 2016.

[13] J. Johnson, R. Bründlinger, C. Urrego, R. Alonso, "Collaborative Development Of Automated Advanced Interoperability Certification Test Protocols For PV Smart Grid Integration," in *EU PVSEC*, Amsterdam, Netherlands, 22-26 Sept 2014.

[14] D. Rosewater, J. Johnson, M. Verga, R. Lazzari, C. Messner, R. Brndlinger, K. Johannes, J. Hashimoto, K. Otani, "International development of energy storage interoperability test protocols for renewable energy integration," in *EU PVSEC*, Hamburg, Germany, 14-18 Sept 2015.

[15] NERC, "1200 MW Fault Induced Solar Photovoltaic Resource Interruption Disturbance Report," North American Electric Reliability Corporation, Tech. Rep., June 2017.

[16] UL-1741 Ed. 2, "Inverters, Converters, Controllers and Interconnection System Equipment for use with Distributed Energy Resources," Underwriters Laboratories, Standard, 2016.

[17] J. Johnson, B. Fox, "Automating the Sandia Advanced Interoperability Test Protocols," in *40th IEEE PVSC*, Denver, CO, 8-13 June 2014.

[18] IEEE Std 1459, "IEEE Trial-Use Standard Definitions for the Measurement of Electric Power Quantities Under Sinusoidal, Nonsinusoidal, Balanced, or Unbalanced Conditions," Institute of Electrical and Electronics Engineers, Inc. New York, NY, Standard, Approved 30 January 2000.

[19] George M. Phillips, *Interpolation and Approximation by Polynomials*. Springer, 2003.

[20] J. Alan V. Oppenheim, Ronald W. Schafer, *Discrete-Time Signal Processing*, 3rd ed. Prentice Hall, 1999.